



Correlation Scales of the Turbulent Cascade at 1 au

Charles W. Smith¹, Bernard J. Vasquez¹, Jesse T. Coburn², Miriam A. Forman³, and Julia E. Stawarz⁴

¹ Physics Department and Space Science Center, Institute for the Study of Earth, Oceans, and Space, University of New Hampshire, Durham, NH, USA
Charles.Smith@unh.edu, Bernie.Vasquez@unh.edu

² Dipartimento di Fisica, Università della Calabria, I-87036 Rende (CS), Italy; jessecob13@gmail.com

³ Department of Physics and Astronomy, State University of New York at Stony Brook, Stony Brook, New York, USA; Miriam.Forman@sunysb.edu

⁴ Department of Physics, Imperial College London, London, UK; J.Stawarz@imperial.ac.uk

Received 2017 October 3; revised 2018 March 14; accepted 2018 March 29; published 2018 April 27

Abstract

We examine correlation functions of the mixed, third-order expressions that, when ensemble-averaged, describe the cascade of energy in the inertial range of magnetohydrodynamic turbulence. Unlike the correlation function of primitive variables such as the magnetic field, solar wind velocity, temperature, and density, the third-order expressions decorrelate at a scale that is approximately 20% of the lag. This suggests the nonlinear dynamics decorrelate in less than one wavelength. Therefore, each scale can behave differently from one wavelength to the next. In the same manner, different scales within the inertial range can behave independently at any given time or location. With such a cascade that can be strongly patchy and highly variable, it is often possible to obtain negative cascade rates for short periods of time, as reported earlier for individual samples of data.

Key words: Sun: heliosphere – magnetic fields – magnetohydrodynamics (MHD) – solar wind – turbulence

1. Introduction

Although there remains a strong tendency to describe solar wind fluctuations as a collection of waves of varying modes (Coleman 1966; Belcher & Davis 1971; Bale et al. 2005; Roberts et al. 2015, 2017), there is a growing recognition that solar wind fluctuations are interacting and evolving nonlinearly in a manner that is most often described as turbulent (Coleman 1968; Matthaeus & Goldstein 1982; Smith 2009; Matthaeus & Velli 2011; Narita et al. 2011; Bruno & Carbone 2013). Whether the turbulence is analogous to hydrodynamic (HD) turbulence, more correctly described as interacting waves (so-called “weak turbulence theory”), or a hybrid of the two remains a topic of debate (Goldreich & Sridhar 1995; Bale et al. 2005; Sahraoui et al. 2009, 2010; Narita et al. 2011; Smith et al. 2012; Alexandrova et al. 2013; Roberts et al. 2015, 2017).

While the precise dynamics responsible for the turbulent evolution of interplanetary fluctuations remains a source of debate, the identities of the spectral subranges are generally agreed upon. At the largest scales, which are typically distances greater than 4.5×10^6 km, and spacecraft-frame frequencies $f_{sc} < 10^{-4}$ Hz at 1 au, variations in the measured plasma parameters are thought to originate with the Sun in combination with dynamics like compression and large-scale shear (e.g., Matthaeus & Goldstein 1986; Zank et al. 1996; Smith et al. 2001a, 2006b, 2011; Tessein et al. 2011). This variability, or fluctuation at the largest scales, is seen to be long-lived on the scale of multiple au. This includes wind shear that is derived from stream interactions, shocks, and coronal mass ejections (CMEs). This is typically called the “energy-containing range” and is the source of energy that forms the spectrum at higher frequencies (Matthaeus et al. 1994).

At smaller scales, the fluctuations are argued to originate within the solar wind by nonlinear processes that remake the fluctuation energy according to the nonlinear dynamics of turbulence. Any energy at these scales that may have originated at the Sun is argued to be converted via nonlinear processes into some other form of fluctuation (other wave modes,

turbulent eddies, etc.). Scales smaller than the energy-containing range and greater than the proton inertial scale or proton Larmor radius form the inertial range that is the most extensively studied portion of the interplanetary spectrum (e.g., Belcher & Davis 1971; Matthaeus & Goldstein 1982; Tessein et al. 2009; MacBride et al. 2010; Bruno & Carbone 2013). It is the dynamics of these and smaller scales that are most in question at the present time. The scale that marks the transition between the energy-containing and inertial scales is generally associated with the correlation scale.

The turbulent cascade of energy through the inertial range of energy-conserving dynamics results in dissipation at scales comparable to the proton gyroradius or ion inertial scale (Behannon 1978; Goldstein et al. 1994; Leamon et al. 1998a, 1998b, 1998c, 1999, 2000; Smith et al. 2001b, 2006a; Hamilton et al. 2008; Markovskii et al. 2008; Bourouaine et al. 2012; Chen et al. 2014). This forms the dissipation range, which is more correctly now called the “ion dissipation range.” The rate of energy cascade in the inertial range can be measured directly by the application of the mixed, third-order structure functions (Politano & Pouquet 1998a, 1998b; MacBride et al. 2005, 2008; Sorriso-Valvo et al. 2007; Marino et al. 2008, 2011, 2012; Stawarz et al. 2009; Coburn et al. 2012; Hadid et al. 2017). The measured energy cascade leads to dissipation at ion scales, which depends on solar wind conditions, and is in good agreement with the measured heating of the thermal protons (Vasquez et al. 2007; Stawarz et al. 2009; Coburn et al. 2012; Hadid et al. 2017). Likewise, turbulent transport theory that is based on turbulence scaling laws has reproduced the observed heating rate for thermal protons from 0.3 to 100 au (Zhou & Matthaeus 1990a, 1990b; Matthaeus et al. 1994, 1999; Zank et al. 1996, 2012; Smith et al. 2001a, 2006b; Isenberg et al. 2003, 2010; Breech et al. 2005, 2008, 2009a, 2009b; Isenberg 2005; Usmanov & Goldstein 2006; Ng et al. 2010; Oughton et al. 2011; Usmanov et al. 2011, 2012, 2014, 2016; Adhikari et al. 2015a, 2015b). At still smaller scales, there is evidence of a second inertial range

and, ultimately, energy dissipation by electron dynamics (e.g., Alexandrova et al. 2009).

The common theories for the dynamics of energy cascade in a turbulent fluid are based upon the power spectrum of the fluctuations and suggest a steady-state cascade of energy through the inertial range (Kolmogorov 1941a; Iroshnikov 1964; Kraichnan 1965; Shebalin et al. 1983; Higdon 1984; Goldreich & Sridhar 1995; Boldyrev 2005, 2006; Smith 2009). However, these theories are all based on specific dynamical processes. A more general description of the turbulent cascade is available from third-moment theory, which is derivable from basic statistical properties (homogeneity, incompressibility, scale separation, and isotropy or another geometry). The derivable third-moment expressions yield a correct analysis of the turbulent cascade regardless of the underlying physical processes. Third-moment theory yields an expected linear function of measurement lag (separation) when the turbulence is stationary that is consistent with the same value of energy transport at all scales within the inertial range. Recent examination of the third-order structure functions that describe the energy cascade in the inertial range have revealed linear functions of lag with strong variation between independent samples that are separated by one or more correlation lengths of the primitive variables (magnetic field, solar wind velocity, and proton density; Coburn et al. 2014, 2015). The implication is that relatively short data intervals are demonstrating a turbulent cascade that is independent from neighboring samples.

Despite the variation, the computed third-order structure functions for individual intervals are seen to have linear scaling in lag over inertial-range scales as predicted by the theory. The variability of measured third-order structure functions between samples of a correlation length or longer is not simply a matter of convergence due to noise in the measurement. The linear scaling of individual samples indicates there is a true variability of local cascade conditions. Convergence to a mean cascade rate requires significantly more data (Podesta et al. 2009). The observed variability of the cascade rate shows that the energy cascade at any given time can be either positive or negative, indicating energy transport to smaller or larger scales, respectively. This strongly suggests that the internal dynamics of solar wind turbulence are, in fact, spotty and perhaps describable as intermittent, depending on the definitions that are used (Kolmogorov 1962; Burlaga 1991; Sorriso-Valvo et al. 1999). Sustained negative-valued energy cascade rate to large scales would result in reduced heating of the thermal population and transfer of energy to larger scales and bring into question what can serve as the energy reservoir for such a process.

This raises critical questions regarding the nature of the energy cascade in the inertial range, the time and spatial scales over which the cascade dynamics change, and possible nonuniformity throughout the inertial range at any given point in space and time. Specifically, we ask whether the energy transport dynamics change only over scales comparable to or greater than the correlation scale of the primitive fluctuations, or is the scale of variation dependent upon the choice of particular scale within the inertial range of the turbulence? In addition, do all inertial-range scales exhibit the same energy transport at any given point in time for a given sample of data? One way to gain insight into these questions is to measure the correlation scale for the cascade dynamics and determine whether the energy cascade is correlated across different spatial

scales in the inertial range. We seek to provide insight into these questions by computing the correlation function for the energy cascade dynamics as described by the third-order expressions.

2. Theory

Here we define the autocorrelation function and turbulent cascade rates as computed from mixed, third-order expressions.

2.1. Autocorrelation Function

Correlation functions provide a measurement of the dependence or independence of measured variables subject to separation in space and time. Autocorrelation functions provide the same measurement of a single variable at two different points. Homogeneous turbulence is defined by correlation functions that are independent of absolute location while maintaining dependence on relative spatial separation. Stationary turbulence is defined by correlation functions that are independent of absolute time while maintaining dependence on relative temporal separation.

We define the autocorrelation function of an observable F to be

$$A(F(\mathbf{x}, t), F(\mathbf{x}', t')) \equiv \langle F(\mathbf{x}', t')F(\mathbf{x}' + \mathbf{x}, t' + t) \rangle_{\text{ensem}}, \quad (1)$$

where $\langle \dots \rangle_{\text{ensem}}$ denotes an ensemble average of similarly prepared samples. We will focus on fluctuations in the observables, so we can write

$$\delta F \equiv F - F_{\text{mean}}. \quad (2)$$

How the average of F , F_{mean} , is best computed is the subject of some debate in the community and will be discussed below. Assuming homogeneity, and if we assume both measurements are made at the same point in time, A becomes a function of relative separation only. We can then define $\delta \mathbf{x} \equiv (\mathbf{x} - \mathbf{x}')$ and write

$$A(\delta F, \delta \mathbf{x}) = \langle \delta F(\mathbf{x}')\delta F(\mathbf{x}' + \delta \mathbf{x}) \rangle_{\text{ensem}}, \quad (3)$$

where $A(\delta F, \delta \mathbf{x})$ is assumed to no longer be a function of \mathbf{x}' .

We will use *Advanced Composition Explorer (ACE)* single-spacecraft data at a fixed cadence (the time between measurements) of 64 s, apply the Taylor frozen-in-flow assumption (Taylor 1938), and assume the turbulence is both stationary and homogeneous. The Taylor assumption states that the time to convect the measurement past the spacecraft is short compared to the time required to evolve the measured variables. This is equivalent to assuming that the measurements are made at a single point in time and many points in space even though the operational reality is the reverse of this. The measurements are one-dimensional time series recorded along the solar wind velocity at a prescribed cadence allowing the above ensemble average to be replaced by a simple average over the time series $\langle \dots \rangle_t$. If we label the data points F_n according to their position in the time series, $n = 1, 2, \dots, N$, we can rewrite Equation (3) as

$$\begin{aligned} A(\delta F, \delta \mathbf{x}) &\simeq \langle \delta F(\mathbf{x}')\delta F(\mathbf{x}' + \delta \mathbf{x}) \rangle_t \\ &= \frac{1}{(N - \delta n)} \sum_{n=1}^{N-\delta n} \delta F(n)\delta F(n + \delta n). \end{aligned} \quad (4)$$

Hereafter, we will omit the subscript on $\langle \dots \rangle$ whenever the expressions apply equally to both ensemble and time averages. We will apply Equation (4) to a variety of measurements, including the magnetic field, solar wind velocity, and thermal proton density and temperature. We will also apply this formalism to compute the correlation function and correlation length of the third-order expressions that describe the cascade of energy through the inertial range of the turbulence.

From this point on, we will interchangeably use the separation according to the data index, δn , and the physical separation given by the Taylor frozen-in-flow assumption, $\delta \mathbf{x} = \mathbf{V}_{\text{SW}} \delta t$, where V_{SW} is the solar wind speed and δt is the separation in time between two arbitrary measurements in the time series. Note that this separation in time represents the relative separation associated with the convection of the solar wind over the spacecraft and does not represent two different times in the evolution of the turbulent system. If we set the cadence of the measurements to be τ , then $\delta t = (\delta n) \tau$. In this analysis, $\tau = 64$ s. From here on, we will use δt and δn interchangeably.

There are numerous ways to apply the concept of Equation (4). When addressing the correlation of the fluctuations relative to the mean, there are currently debates on what is an appropriate definition of “mean.” Traditionally, a relatively large sample of 1 hr or more of data is selected, the mean of that sample is computed, the mean is subtracted from the individual measurements, and the resultant fluctuations are analyzed (e.g., Matthaeus & Goldstein 1982; Hamilton et al. 2008). We will describe our approach to the calculation of the mean in the analysis below.

It still becomes necessary to perform an ensemble average to obtain $A(\delta F, \delta n)$ from individual estimates, so in the past, we subset the data into subintervals that are a correlation length or more in duration for the primitive variables (Coburn et al. 2014, 2015) in order to obtain uncorrelated estimates for building an ensemble of independent estimates of A . The average over the resulting estimates yields the statistical average of $A(\delta F, \delta n)$. Using subintervals that are shorter than a correlation length would imply an interdependence of sequential estimates that would require a more complex statistical theory. Independent estimates allow us to use Gaussian statistics to compute means and uncertainties when addressing the ensemble average.

Several quantities of immediate use are made available by this analysis. When addressing fluctuations, the correlation function at zero lag is the variance of the fluctuations. Its value can depend upon the length of data used to determine the mean as the averaging process exchanges energy between the locally computed mean and the fluctuation. We can quantify the correlation scale that characterizes the distance over which the measurement decorrelates in several ways (Batchelor 1953; Matthaeus et al. 1999). The standard definition for the correlation scale is the integral under the correlation function divided by the variance,

$$\lambda_c^i \equiv \sum_{\delta n=0}^N A(\delta F, \delta n) / A(\delta F, \delta n = 0), \quad (5)$$

where this definition is only valid if the computed λ_c^i is shorter than the maximum lag of the analysis where $A(\delta F, N) \simeq 0$. Some correlation functions shown here do not extend to sufficient lags, so we also use an alternative definition that the correlation length, λ_c^e , is the lag where $A(\delta F, \lambda_c^e) = A(\delta F, \delta n = 0) / e$ and

$e = 2.71828\dots$ As a practical matter, the correlation scale offers an objective determination of the large-scale limit for the inertial range of the primitive variables. Larger scales are more correctly associated with the so-called “energy-containing range” that provides the energy reservoir to drive the turbulence.

2.2. Third-order Expressions

It is possible to derive a statistical expression to compute the rate of energy transport through the inertial range for isotropic, homogeneous, stationary, incompressible turbulence. If we first consider Navier–Stokes HD flow, von Karman & Howarth (1938) demonstrated that the statistical correlations in HD flow could be expressed in a generalized tensor form. Kolmogorov (1941b) realized that if the flow exhibited scale separation such that there exists an inertial range where energy transport is energy conserving and a separate dissipation scale where energy is dissipated, then it is possible to derive an expression without additional approximation that yields the average rate of energy transport through the inertial range and, hence, the rate of energy dissipation. This is his so-called “Four-Fifths Law” of incompressible HD. We write this in a manner to explicitly acknowledge the ensemble average:

$$S_3^{\text{HD}}(\mathbf{L}) \equiv [V_L(\mathbf{x} + \mathbf{L}) - V_L(\mathbf{x})]^3 \quad (6)$$

and

$$\langle S_3^{\text{HD}}(\mathbf{L}) \rangle = -(4/5) \epsilon^{\text{HD}} |\mathbf{L}|, \quad (7)$$

where V_L is the component of the flow velocity along the separation vector \mathbf{L} and ϵ^{HD} is the scale-independent rate of energy transport through the inertial range. Hereafter, we will refer to terms like Equation (6) as “third-order expressions,” as they are only structure functions in the formal sense when averaged over an ensemble as in Equation (7). The ensemble average contained in Equation (7) is critical to the definition of ϵ^{HD} , as the derivation requires the application of symmetry arguments that may not be point-wise valid. Equation (7) is similar to a related third-order expression derived by Yaglom (1949).

This third-order expression has been generalized for application to magnetohydrodynamic (MHD) flow (Politano & Pouquet 1998a, 1998b),

$$D_3^{\pm}(\mathbf{L}) \equiv \Delta Z_L^{\mp}(\mathbf{L}) \sum_i [\Delta Z_i^{\pm}(\mathbf{L})]^2 \quad (8)$$

and

$$\langle D_3^{\pm}(\mathbf{L}) \rangle = -(4/3) \epsilon_{\text{MHD}}^{\pm} L, \quad (9)$$

where

$$\mathbf{Z}^{\pm} \equiv \mathbf{V} \pm \mathbf{B} / \sqrt{(4\pi\rho)} \quad (10)$$

defines the Elsässer variables (Elsässer 1950). We use the instantaneous density to compute \mathbf{Z}^{\pm} , although in past studies averaging over 1–12 hr samples we found no significant difference if we used the average density to compute \mathbf{Z}^{\pm} . The variable Z_L is the component of \mathbf{Z} along the separation vector \mathbf{L} , and

$$\Delta \mathbf{Z}(\mathbf{x}, \mathbf{L}) \equiv \mathbf{Z}(\mathbf{x}) - \mathbf{Z}(\mathbf{x} + \mathbf{L}). \quad (11)$$

In keeping with the convention of the original derivation,

$$\epsilon_{\text{MHD}}^{\text{tot}} = (\epsilon_{\text{MHD}}^+ + \epsilon_{\text{MHD}}^-)/2 \quad (12)$$

is the total energy cascade for the turbulent system.

Unlike the questions surrounding the computation of correlation functions, Equation (9) can be evaluated without subtraction of a local mean. The term ΔZ automatically subtracts the local mean in a manner prescribed by a first-principles derivation.

In order to better understand the underlying correlations of the terms in Equation (9), we can define an expression at each point n in the series and a fixed lag λ :

$$D_3^\pm(n, \lambda) = [Z_L^\mp(n) - Z_L^\mp(n + \lambda)] \times \sum_{i=1}^3 [Z_i^\pm(n) - Z_i^\pm(n + \lambda)]^2. \quad (13)$$

The distinction between λ above and δn in the autocorrelation function expressions is made to facilitate the computation of the autocorrelation function of $D_3^\pm(\lambda)$. As with δn , time separation associated with the lag in the third-order expression is given by $\delta t = \lambda\tau$, and spatial separation is given by $L = \tau\lambda V_{\text{SW}}$. We evaluate L for the purpose of computing ϵ by using the value of V_{SW} averaged for the two lagged points in ΔZ^\pm . In keeping with Equation (12), we can define an averaged third-order function at each point in the data:

$$D_3^{\text{tot}}(n, \lambda) = (D_3^+(n, \lambda) + D_3^-(n, \lambda))/2. \quad (14)$$

By definition, Equations (13) and (14) lack the statistical properties that are assumed for the turbulent cascade including homogeneity. We can average Equation (13) over sufficient data to reclaim those statistical properties,

$$\langle D_3^\pm(\lambda) \rangle_t = \frac{1}{(N - \lambda)} \sum_{n=1}^{N-\lambda} D_3^\pm(n, \lambda) \quad (15)$$

$$= \frac{1}{(N - \lambda)} \sum_{n=1}^{N-\lambda} \left\{ \Delta Z_L^\mp(n, \lambda) \sum_{i=1}^3 [\Delta Z_i^\pm(n, \lambda)]^2 \right\}, \quad (16)$$

and from this we can compute ϵ^\pm . The same applies to the ensemble average of Equation (14).

It is well established that a fundamental asymmetry exists in the solar wind between Z^\pm , wherein there is typically greater energy in the outward (anti-sunward) propagating component. Since the propagation direction of Z^\pm is defined relative to the mean magnetic field, we can define $Z^{\text{out/in}}$ according to the local sector type where Z^+ (Z^-) propagates sunward (anti-sunward) in an away sector field and anti-sunward (sunward) in a toward sector field. We will refer to anti-sunward propagation by Z^{out} and sunward propagation by Z^{in} , and in some instances, we will gather statistics according to this definition.

It should be noted that Equations (7), (9), and 16 are derived for isotropic turbulence while solar wind turbulence is well known to be highly anisotropic (Belcher & Davis 1971; Matthaeus et al. 1990). Very similar expressions for two-dimensional (2D) turbulence and turbulence that is a combination of 2D and field-aligned have been derived and analyzed (MacBride et al. 2005, 2008; Smith et al. 2009, 2010; Stawarz et al. 2009, 2010, 2011; Forman et al. 2010; Coburn et al. 2012, 2014, 2015). We will present an analysis of these slightly simpler isotropic expressions so as not to unduly complicate the discussion.

The third-order formalism described above is completely general subject to the stated assumptions of incompressibility, homogeneity, stationarity, isotropy, and scale separation. For some purposes, any of the above assumptions can be argued to be invalid in the solar wind, but this represents a good starting point from which to examine the correlation scale of turbulent processes. The expressions are valid regardless of the nonlinear dynamics active in the turbulent cascade and are derived without regard to specific wave modes.

3. Data Analysis

We focus on a single solar rotation of solar wind data recorded by the *ACE* spacecraft (Garrard et al. 1998; McComas et al. 1998; Smith et al. 1998; Stone et al. 1998). There is nothing unique about this rotation. The measurements were recorded shortly after the peak activity of solar maximum. The interval contains shocks and assorted variations in solar wind conditions that provide a good sample of the diverse conditions for solar wind turbulence at 1 au.

3.1. Primitive Variables

A well-known problem with measuring correlation lengths in the solar wind derives from the fact that there is substantial power in fluctuations at arbitrarily long timescales. Attempts to measure the correlation length for the primitive variables such as magnetic field, velocity, and density fluctuations associated with interplanetary turbulence can be influenced by stream structure, sector structure, solar rotation, and even the solar cycle. Past attempts to overcome this problem place the correlation length for the turbulence at between 30 minutes and several hr (Fisk & Sari 1973; Matthaeus et al. 1999, 2005; Dasso et al. 2008; Matthaeus et al. 2010).

We illustrate this fact by selecting a solar rotation from the *ACE* catalog that has good data coverage and a range of flow conditions (Garrard et al. 1998; McComas et al. 1998; Smith et al. 1998; Stone et al. 1998). We choose solar rotation 2303 that extends from day of year (DOY) 101 to 127 of 2002 and use the merged MAG and SWEPAM data set with $\delta t = 64$ s resolution. We select data in heliocentric *RTN* coordinates, where the radial component R extends from the Sun to the spacecraft, the azimuthal component T is coplanar to the Sun's rotational equator and directed in the sense of rotation, and the normal component $N = \mathbf{R} \times \mathbf{T}$. This is the same coordinate system in which Parker first defined the spiraling heliospheric magnetic field (Parker 1961, 1963). When applying the expressions derived above, the direction of positive lag L is equivalent to the $-R$ component, which opposes the solar wind flow.

Figure 1 shows the data used in this analysis. The plot is made using data from the MAG and SWEPAM instruments with a common 64 s resolution for Carrington solar rotation 2303 extending from DOY 101 to 127 of 2002. The SWEPAM data have a natural 64 s cadence, while the MAG data are collected at 3 s^{-1} and averaged to the 64 s cadence of SWEPAM via an intermediate 16 s average. The top three panels show the field intensity; the magnetic field north/south elevation angle $\delta \equiv \tan^{-1}(B_N/B_L)$, where $B_L \equiv \sqrt{B_R^2 + B_T^2}$; and the magnetic field azimuthal angle $\Theta \equiv \tan^{-1}(B_T/B_R)$. Both Θ and δ are given in degrees computed in (R, T, N) coordinates. Here V_R , V_T , and V_N are the three components of the wind velocity in heliocentric (R, T, N) coordinates; N_P is the

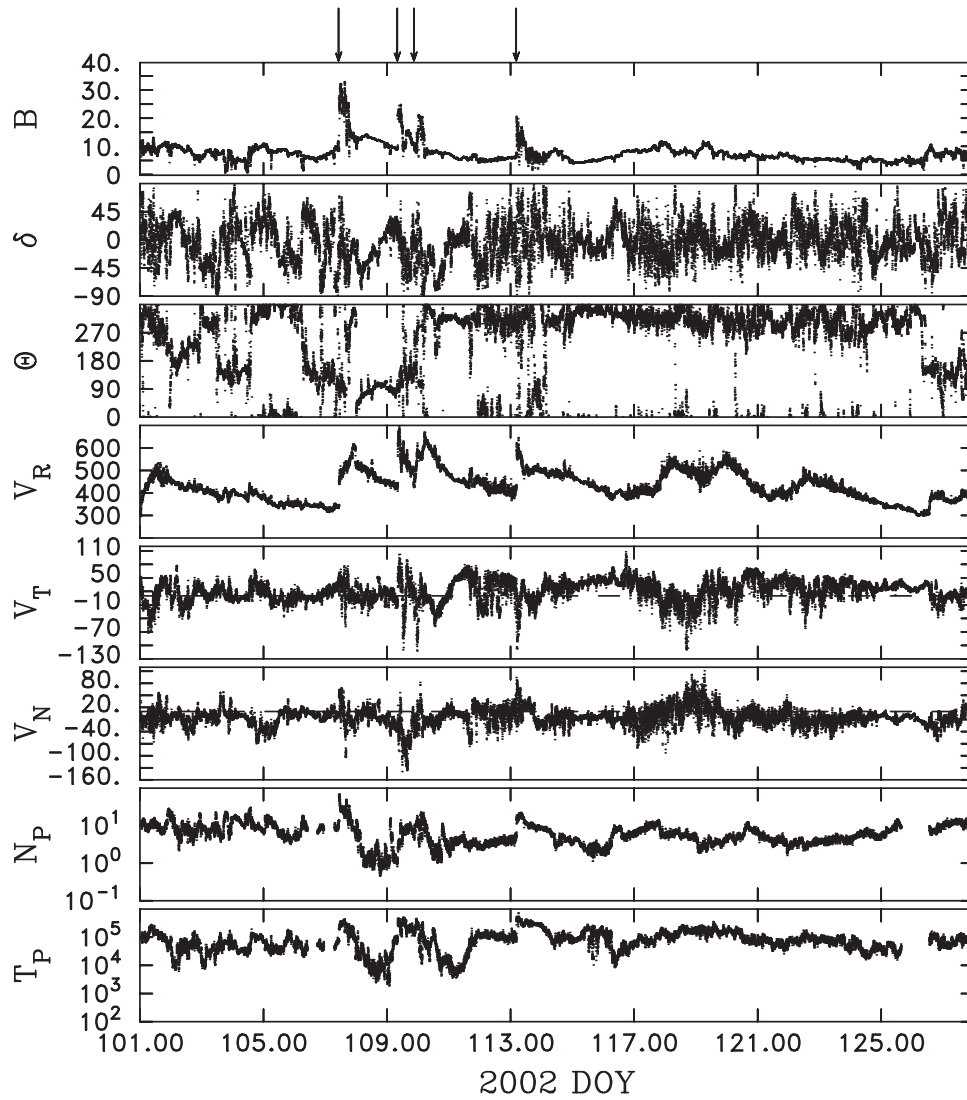


Figure 1. Observations by the *ACE* spacecraft of solar wind plasma conditions for solar rotation 2303 extending DOY 101–127 of 2002. Top to bottom: magnetic field intensity B in nT; magnetic field north/south elevation angle δ in deg; magnetic field azimuthal angle Θ in deg; radial, tangential, and normal component of the solar wind velocity; proton density N_p in cm^{-3} ; and proton temperature T_p in K. The arrows above the top panel mark the locations of four shocks. See text for further description.

Table 1
Recorded Shocks Evident in Figure 1

| DOY::Hour:Min [UT] | Exclusion [UT] | F/R | r_N | Θ_{Bn} [deg] | M_A |
|-----------------------|-----------------------|-----|---------------|-------------------------|---------------|
| 107::10:21 | 106::22:21–108::22:21 | F | 3.4 ± 0.1 | $90^\circ \pm 1^\circ$ | 2.2 ± 0.4 |
| 109::08:02 | 108::20:02–110::20:02 | F | 2.4 ± 0.5 | $67^\circ \pm 6^\circ$ | 1.6 ± 0.4 |
| 109::20:50 | 109::08:50–111::08:50 | F | 1.2 ± 0.1 | $53^\circ \pm 20^\circ$ | 2.0 ± 0.5 |
| 113::04:15 | 112::16:15–114::16:15 | F | 3.0 ± 1.1 | $25^\circ \pm 8^\circ$ | 3.7 ± 0.7 |

Note. Here F denotes a forward shock (no reverse shocks were evident in this solar rotation), r_N is the compression ratio of the shock, Θ_{Bn} is the angle between the shock normal and the upstream magnetic field, and M_A is the Alfvénic Mach number.

measured proton density; T_p is the measured proton temperature; and $V_{SW} = \sqrt{V_R^2 + V_T^2 + V_N^2}$ defines the wind speed. Throughout the paper, we use units of nT for magnetic field, km s^{-1} for speed, cm^{-3} for density, and K for temperature.

There are four shocks cataloged for this solar rotation and marked by arrows above the top panel of Figure 1. Although Figure 1 would seem to show two additional shocks on DOYs 117 and 127, careful examination of the data does not support

this interpretation. Table 1 lists the shock times and general characteristics, where the shocks are determined to be either forward (F) or reverse (R). The table lists the shock compression ratio $r_N \equiv \rho_d/\rho_u$, where ρ_d (ρ_u) is the proton density downstream (upstream) of the shock; the angle between the computed shock normal and upstream magnetic field direction Θ_{Bn} ; and the Mach number of the shock $M_A = V_S/V_A$, where V_S is the shock speed in the plasma

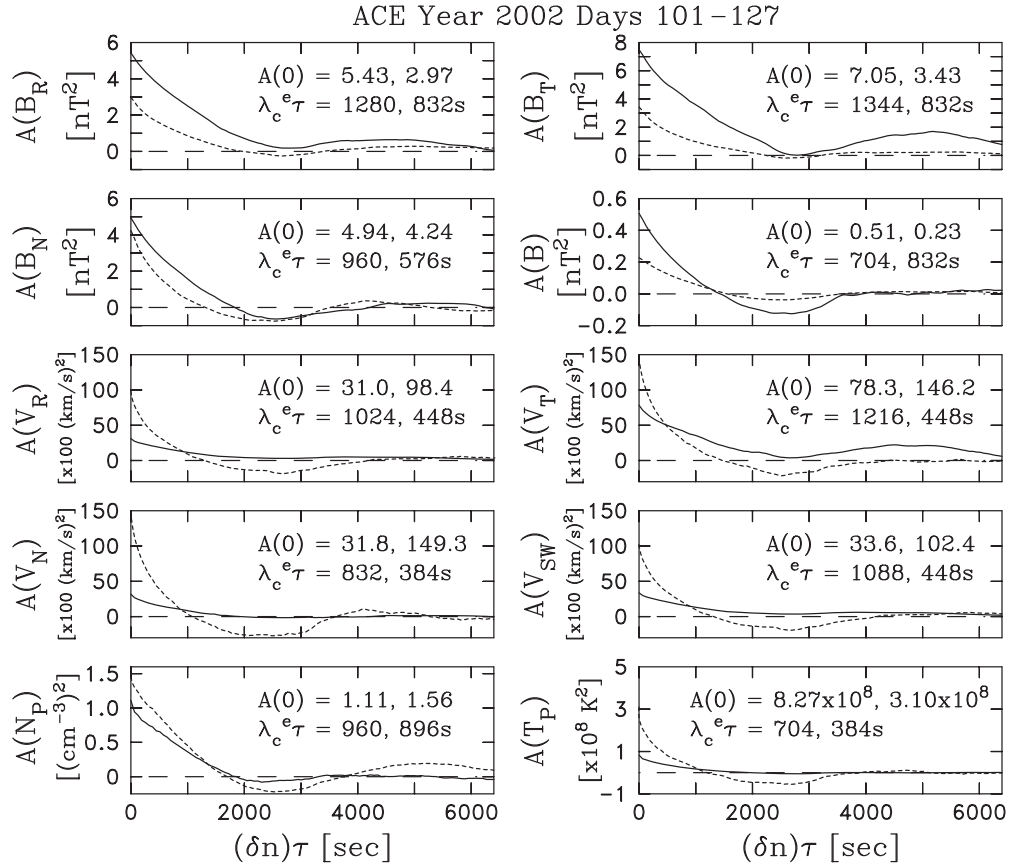


Figure 2. Correlation function for fluctuations in the primitive variables computed in the traditional manner for toward sectors (solid curves) and away sectors (dashed curves). Left to right and top to bottom, they represent the variables B_R , B_T , B_N , B_{mag} , V_R , V_T , V_N , V_{SW} , N_P , and T_P . The correlation functions both here and below are computed using Equation (4). The value of the correlation function at zero lag, $A(\delta F(0))$, is the variance for each variable analyzed, and the correlation lengths are given in each panel (left to right) for toward and away sectors.

frame. The computation of shock properties is performed using the Rankine–Hugoniot shock conditions (Boyd & Sanderson 1969) and an adaptation of the method developed by Viñas & Scudder (1986), Szabo (1994), and Vorotnikov et al. (2008, 2011). The shock crossings are clearly evident in Figure 1, where both B and V_R increase at the shock while the magnetic field and flow are redirected after the shock passage, magnetic fluctuation level, proton density, and proton temperature rise downstream. Shocks, their foreshocks, and their drivers are eliminated from our analyses throughout this paper by excluding any data from 12 hr before the shock until 36 hr after the shock crossing. Because the first three shocks occur in close proximity, this removes 154 hr and 29 minutes of data from the analysis. There are ~ 20.5 days of remaining data in this solar rotation. Allowing for missing data and requiring that all primitive variables be available for any given time to perform the analyses described here, there are 24,417 data points analyzed here.

We first compute the correlation functions using those 20 days of primitive variables. We focus on the three components of the magnetic field (B_R , B_T , B_N), the field magnitude B , the three components of the solar wind velocity (V_R , V_T , V_N), the proton density N_P , and the proton temperature T_P . We include T_P even though it is not used elsewhere in this analysis. The correlation function $A(\delta F, \delta t)$ is computed using Equation (4) out to a lag of 100 points ($\delta n = 100$ points, $\delta t = 6400$ s). A maximum lag of 100 points $\simeq 1.8$ hr, which is comparable to or exceeds the generally agreed-to range of

correlation lengths for primitive variables in the solar wind. The function $A(\delta F, \delta t)$ requires that we use fluctuations of the primitive variables. To obtain estimates of the means, we use a sliding average of N_{mean} points centered on each data point. Points near the beginning or end of the solar rotation and points near the boundaries of excluded data involving shocks and their drivers use asymmetric means so that the number of available data points is preserved by the averaging process. We have done this using several (odd) values for N_{mean} and will compare those results below. Averages and differences across the heliospheric current sheet are not permitted, as this would artificially increase the fluctuation. Therefore, we compute A for primitive variables in the toward and away sectors separately. This produces a data set that retains the 64 s cadence of the original but with local mean values subtracted.

The evaluation of $A(\delta F, \delta t)$ is obtained using Equation (4) without any intermediate averaging of the estimates. We show the computed results in Figure 2, where solid lines represent toward sectors and dashed lines represent away sectors. In this instance, we use $N_{mean} = 101$ points ($N_{mean} \tau = 6464$ s). Both the values of the correlation functions at zero lag $A(\delta F, \delta t = 0)$ (the variance) and the correlation scales computed using the e -folding method are listed on the panels. Note that the measured correlation length is in all cases shorter than the 100 point = 6400 s maximum lag. Values vary from 384 to 1344 s with a resolution of 64 s due to the analysis method. Values of the correlation scale derived from the integration method are comparable and listed in Table 2.

Table 2
Parameters from Figure 2

| A | Sector T/A | $A(0)$ | $\lambda_c^e \tau$ (s) | $\lambda_c^i \tau$ (s) |
|-------------|---------------|--------|---------------------------|---------------------------|
| $A(B_R)$ | T | 5.43 | 1280 | 1356 |
| | A | 2.97 | 832 | 861 |
| $A(B_T)$ | T | 7.05 | 1344 | 1599 |
| | A | 3.43 | 832 | 867 |
| $A(B_N)$ | T | 4.94 | 960 | 667 |
| | A | 4.24 | 576 | 283 |
| $A(B)$ | T | 0.51 | 704 | 294 |
| | A | 0.23 | 832 | 609 |
| $A(V_R)$ | T | 31.0 | 1024 | 1429 |
| | A | 98.4 | 448 | 213 |
| $A(V_T)$ | T | 78.3 | 1216 | 1732 |
| | A | 146.2 | 448 | 238 |
| $A(V_N)$ | T | 31.8 | 832 | 667 |
| | A | 149.3 | 384 | 85 |
| $A(V_{SW})$ | T | 33.6 | 1088 | 1511 |
| | A | 102.4 | 448 | 215 |
| $A(N_P)$ | T | 1.11 | 960 | 686 |
| | A | 1.56 | 896 | 742 |
| $A(T_P)$ | T | 8.27 | 704 | 547 |
| | A | 3.10 | 384 | 107 |

Note. Here T/A denotes toward/away sectors, $A(0)$ is the correlation function value at zero separation, λ_c^e is the exponential definition of the correlation scale, and λ_c^i is the integration definition of the correlation scale.

Several other familiar facts are evident in Figure 2. The variance, $A(0)$, is smaller for B than for the components in keeping with the often-stated claim that magnetic fluctuations are magnitude-conserving. Toward sectors have larger magnetic variances and correlation scales than away sectors, except for B , where the roles of λ_c^e and λ_c^i are reversed. The variance of the solar wind velocity is approximately equal across the components and the magnitude while the away sectors have larger variances and smaller λ_c^e . This holds for λ_c^i as well. The proton density and temperature are very much like every other primitive variable except for one thing: the relative values of the variance and correlation scales for N_P are the same as for the other proton data, while T_P follows the scaling of the magnetic field data.

As stated above, the length of the averaging interval used to compute the fluctuations of the primitive variables has a profound effect on the statistics and correlation of the fluctuations. Figure 3 shows the computed correlation functions for the same variable, B_N , using five different values of $N_{\text{mean}} = 21, 51, 101, 201,$ and 301 points ($N_{\text{mean}} \tau = 1344, 3264, 6464, 12,864,$ and $19,264$ s). Toward and away sectors are again analyzed separately. As N_{mean} increases, energy is transferred from the designated mean to the fluctuation with an increase in both the variance and the correlation scale. While there are varying and subjective opinions on the proper definition for both the mean and the fluctuations, there is no agreed-to formalism. The variability seen here when the averaging interval is altered is an indication of one uncertainty in the overarching question, ‘‘What is the correlation length for primitive variables in the solar wind?’’ That uncertainty is how to correctly define the mean so as to then compute the fluctuations relative to the mean. This is not the case when examining the third-order expressions that describe the

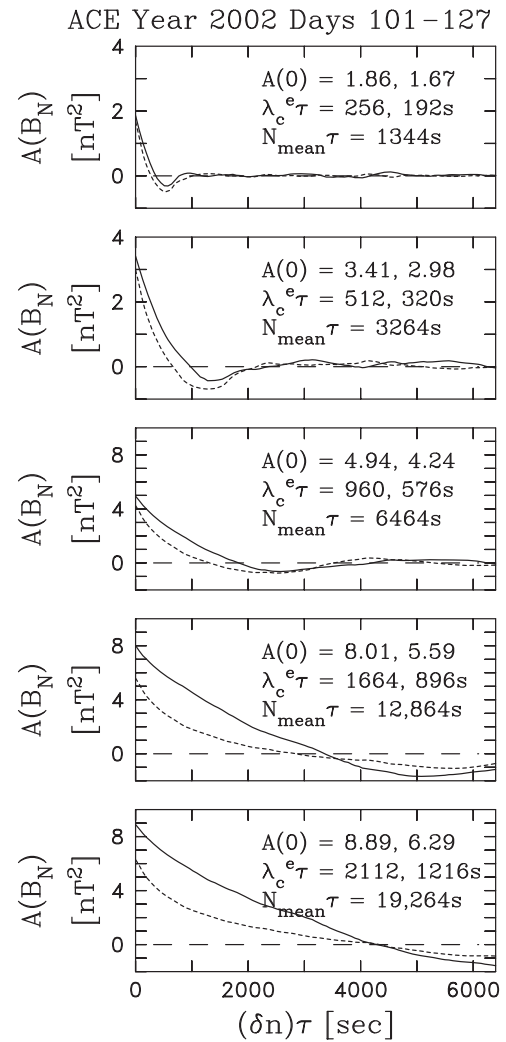


Figure 3. Top to bottom: correlation function for fluctuations in B_N for toward sectors (solid curves) and away sectors (dashed curves) using five values for the local mean analysis: $N_{\text{mean}} = 21, 51, 101, 201,$ and 301 points ($N_{\text{mean}} \tau = 1344, 3264, 6464, 12,864,$ and $19,264$ s). Both the correlation function at zero lag and the correlation length are given for toward sectors (left) and away sectors (right). Variation in the length of the averaging interval leads to an exchange in what is determined as mean and fluctuation. Longer means admit lower-frequency fluctuations into the analysis, resulting in larger variances and longer correlation scales.

turbulent energy cascade because no subjective mean field subtraction is required.

3.2. Energy Cascade

The energy cascade, as described by the ensemble-averaged third-order structure functions, can be taken to predict uniform cascade rates across the inertial-range scales when one also considers the theories of HD cascade rates based on the turbulent power spectrum (Kolmogorov 1941a) and MHD (Iroshnikov 1964; Kraichnan 1965; Zhou & Matthaeus 1989; Goldreich & Sridhar 1995). However, the statistics of these expressions when averaged over 1–3 hr intervals (one or more correlation scales of the primitive variables) have been shown to exhibit large variability with standard deviations an order of magnitude greater than the ensemble-averaged means computed from many hours of data (Coburn et al. 2014, 2015). In HD, the lifetime of a turbulent eddy is one turnover time (one oscillation). A fundamental tenet of weak turbulence theory is

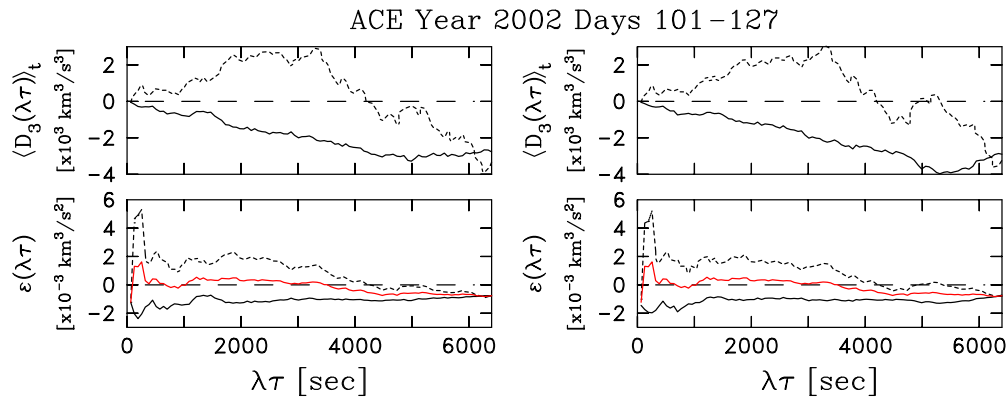


Figure 4. Top left: calculated values of $\langle D_3^+(\lambda\tau) \rangle_t$ (solid curve) and $\langle D_3^-(\lambda\tau) \rangle_t$ (dotted curve). Top right: calculated values of $\langle D_3^{\text{out}}(\lambda\tau) \rangle_t$ (solid curve) and $\langle D_3^{\text{in}}(\lambda\tau) \rangle_t$ (dotted curve). Bottom left: calculated values of ϵ^+ (solid black curve), ϵ^{tot} (red curve), and ϵ^- (dotted curve). Bottom right: ϵ^{out} (solid black curve), ϵ^{tot} (red curve), and ϵ^{in} (dotted curve).

that the timescale at which energy is exchanged between the modes is long compared to the wave period. It therefore becomes difficult to imagine that the variability of the cascade is coherent across the turbulent spectrum over timescales comparable to the correlation scale of the primitive variables if for no other reason than that the transfer of energy to larger scales would deplete whatever energy exists at smaller scales in a relatively short time. Moreover, the disparate life spans of fluctuations at different scales would also require that new small-scale dynamics remain sufficiently in phase so that the energy cascade in the same sense is maintained. Given that energy is transported through the turbulent spectrum at a finite rate and over a finite time, strict agreement between the third-order expressions at all scales and theories based on the turbulent power spectrum (above) would require a very high degree of coherence over many lifetimes of the turbulent fluctuations. The analysis presented here attempts to address these questions. As a practical matter, it is also beneficial to establish the correlation scale for the energy cascade dynamics and compare it to the correlation scale of the primitive variables.

Figure 4 shows Equations (9) and (16) averaged over the solar rotation, with the exclusion of the same data points that were excluded in the above analysis. The functions $\langle D_3^\pm(\lambda\tau) \rangle_t$ possess good linearity for lags up to ~ 3000 s. For the same reason, the functions $\epsilon^{\pm, \text{tot}}(\lambda\tau)$ show nearly constant values over the same range of lags, with some departure from constancy at the smallest scales. A lag of 3000 s is a good assessment of the correlation scale marking the largest scales of the energy-conserving dynamics of the inertial range and the onset of the energy-containing range. The functions $\langle D_3^\pm(\lambda\tau) \rangle_t$ are not predicted to have linear scaling at energy-containing scales, and the functions $\epsilon^{\pm, \text{tot}}(\lambda\tau)$ are not predicted to be constant at these scales. This is easy to understand. If $\langle D_3^\pm(\lambda\tau) \rangle_t$ provides a measure of the energy transport through the scale in question, where energy transport is scale-independent in the inertial range, in the energy-containing range, this measure divides the energy sources into scales that are larger and smaller than the scale in question. If the turbulence provides net transport to smaller scales, then the net average energy transport decreases with increasing scale in the energy-containing range, as few sources are available at increasing scales. It appears that the measurement of $\langle D_3^\pm(\lambda\tau) \rangle_t$ and ϵ may be a good, independent assessment of

the scale demarking the boundary between the energy-containing and inertial ranges.

Coburn et al. (2014, 2015) demonstrated that 1 and 3 hr averages of Equation (9) yield a broad distribution of values with standard deviations a factor of 10 greater than the mean. These two averaging intervals were chosen because of their relationship to the correlation scale for the primitive variables. It is worthwhile here to examine the distribution function for D_3^{tot} defined in Equation (14) when computed at higher time resolution, as these are the values that underpin the above distributions. We choose $\lambda = 5, 10, 25,$ and 100 points ($\lambda\tau = 320, 640, 1600,$ and 6400 s), which samples the range of inertial-range lags available from these data. Figure 5 shows the distribution of values computed for D_3^{tot} using the full 64 s cadence of the data. The 64 s resolution is too coarse to resolve the likely rollover of the distribution at small values where the distribution is expected to be approximately Gaussian. Between 35% and 75% of the data have $|D_3^{\text{tot}}| > 200 \text{ km}^3 \text{ s}^{-1}$ and are off the scale of the plot. We omit these values so that the distribution can be better seen around the value of the mean.

Table 3 lists the mean, $\langle D_3^{\text{tot}} \rangle_t$; standard deviation, σ_{std} ; and error of the mean, σ_M , for each panel in Figure 5. The error of the mean is defined as σ_{std} divided by the square root of the number of correlation lengths in the data. The correlation length is computed below. The means are consistently smaller than the error of the mean, but the purpose of showing this analysis is not to argue that one solar rotation contains enough data to obtain convergence of the mean to a statistical average. The purpose of this analysis is to demonstrate the variability of the measurement and the dependence upon lag. More data that are similarly prepared will reduce the error of the mean, but it is unlikely to significantly alter the computed standard deviation. This, together with the need to select data intervals with comparable wind speed and temperature, offers an explanation of why so many data are required to produce average energy cascade rates that are in agreement with proton heating (Stawarz et al. 2009; Coburn et al. 2012).

We can address the scale at which the above measurements decorrelate simply by evaluating the autocorrelation function for the third-order expressions at a fixed lag. We do this by evaluating Equation (13) as a time series using the primitive

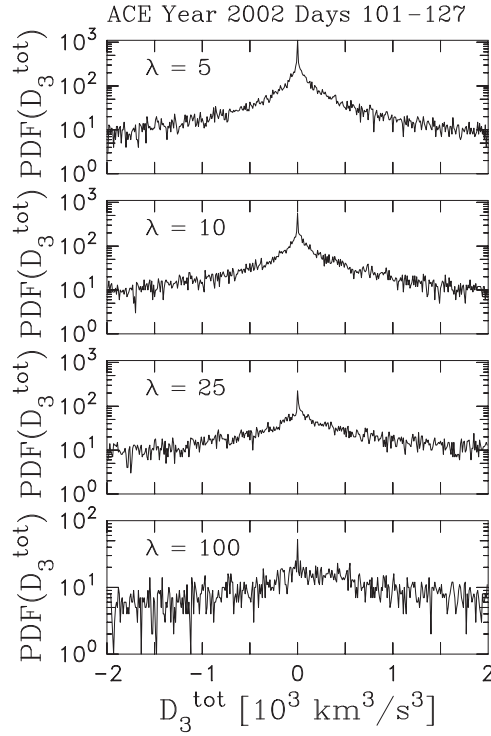


Figure 5. Distribution function for D_3^{tot} computed for four different values of the lag: $\lambda = 5, 10, 25,$ and 100 points ($\lambda\tau = 320, 640, 1600,$ and 6400 s). Note that in each case, the standard deviation σ_{std} is significantly greater than the mean $\langle D_3^{\text{tot}} \rangle$, implying large variations in the cascade rate relative to the average value.

Table 3
Parameters for Figure 5

| λ | $\lambda\tau$ (s) | $\langle D_3^{\text{tot}} \rangle_t$ | σ_{std} ($\text{km}^3 \text{s}^{-3}$) | σ_M |
|-----------|----------------------|--------------------------------------|--|------------|
| 5 | 320 | 82.6 | 2.6×10^4 | 176 |
| 10 | 640 | 29.9 | 3.5×10^4 | 235 |
| 25 | 1600 | 267. | 5.2×10^4 | 354 |
| 100 | 6400 | -3050 | 13.5×10^4 | 941 |

Note. Here λ counts data separation by data points, $\lambda\tau$ counts data separation by time, $\langle D_3^{\text{tot}} \rangle_t$ is the mean of D_3^{tot} , σ_{std} is the standard deviation of D_3^{tot} , and σ_M is the error of the mean of D_3^{tot} .

variables and then computing the correlation function:

$$\begin{aligned}
 A(D_3^{\text{tot}}(\lambda), \delta n) &\equiv \langle D_3^{\text{tot}}(n, \lambda) D_3^{\text{tot}}(n + \delta n, \lambda) \rangle_t \\
 &= \frac{1}{(N - \lambda - \delta n)} \sum_{n=1}^{N - \lambda - \delta n} D_3^{\text{tot}}(n, \lambda) D_3^{\text{tot}}(n + \delta n, \lambda).
 \end{aligned}
 \tag{17}$$

The analysis is the same as was used to prepare Figure 2, but now we use the computed third-order expression at a lag λ as input rather than the primitive variables. Figure 6 shows the result using a lag of $\delta n = 25$ points ($\delta t = 1600$ s). Note the demonstrably shorter correlation scales evident in all Five panels of Figure 6 compared to those seen in Figure 2. Moreover, the correlation lengths vary from 20% to 30% of the lag value.

We can vary the lag used in the analysis. Figure 7 shows the correlation function for D_3^{tot} computed in the same manner using four different values of the lag: $\lambda = 5, 10, 25,$ and

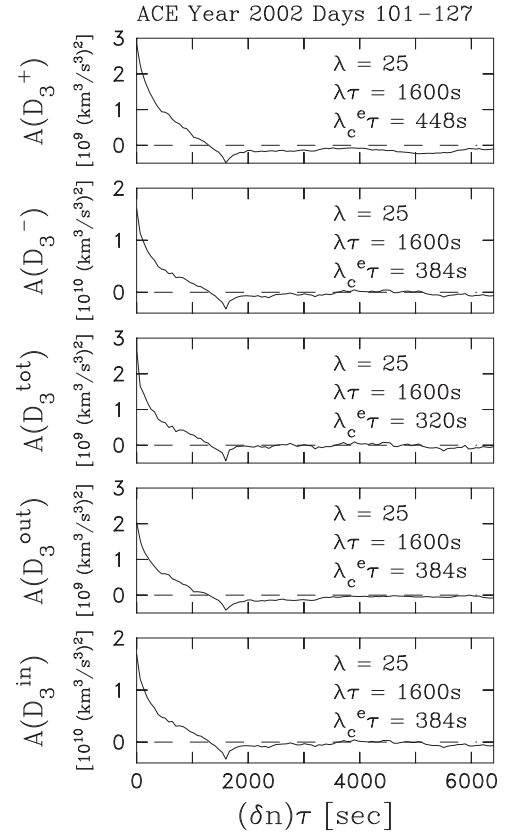


Figure 6. Correlation functions for D_3^{\pm} , D_3^{tot} , and $D_3^{\text{out,in}}$ evaluated at a lag of $\lambda = 25$ points ($\lambda\tau = 1600$ s). The time series for D_3 are computed from the primitive variables. Subtraction of means is unnecessary, as the expressions naturally accomplish this goal. The technique is otherwise identical to that used in Figure 2.

100 points ($\delta t = 320, 640, 1600,$ and 6400 s). Figure 7 (left) shows the analysis of the same data used in Figure 6. In each case, the apparent correlation scale tracks at 20% of the lag value with $\lambda_c^e \simeq \lambda_c^i$ (see Table 4). This means that the third-order expressions decorrelate on the scale of the lag. Unlike the primitive variables, which have correlation scales that are dependent on the scale on which the mean is computed, the third-order expressions decorrelate in a single scale length consistently without regard for any secondary consideration required to compute a mean value. Inertial-range dynamics are coherent over only the scale of interest. In the event that the above conclusions can be traced to the frequent crossings of the heliospheric current sheet, as evidenced in the first half of Figure 1, we offer Figure 7 (right), which uses only data from DOYs 117–124 when the spacecraft is consistently within an away sector region and does not cross the heliospheric current sheet. The results are nearly identical, which indicates that the conclusion that the correlation length scales with the lag is a property of the background turbulence.

3.3. Second-order Expressions

The correlation functions for second-order expressions behave in much the same manner as the equation for the energy cascade. We can take Equation (4) and let $\delta F \equiv [\Delta Z_i^{\pm}(L)]^2$ to compute the correlation function for a second-order expression evaluated at a given lag. Note that ΔZ_i automatically removes the mean from the variable. For simplicity, let us choose the radial component $\Delta Z_R^+(L = \lambda\tau V_{\text{SW}})$. All components of ΔZ^{\pm} behave

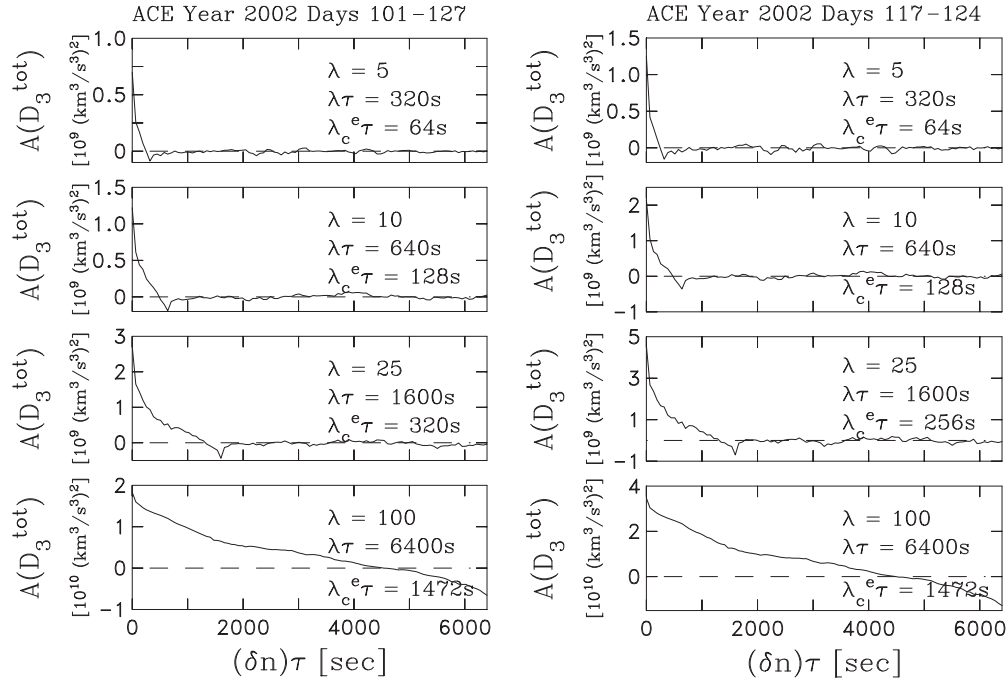


Figure 7. Left: correlation function for D_3^{tot} evaluated at four lags: $\lambda = 5, 10, 25,$ and 100 points ($\lambda\tau = 6400, 1600, 640,$ and 320 s) computed using the same data as in Figure 6. Right: same analysis using only DOYs 117–124. Note that the correlation scale tracks with the lag used in each analysis while the variance (correlation at zero lag) on the right is significantly greater than that on the left. The variance is given in Table 4.

Table 4
Parameters for Figure 7

| λ | $\lambda\tau$ (s) | $A(0)$ | $\lambda_c^e\tau$ (s) | $\lambda_c^i\tau$ (s) |
|-----------|----------------------|----------------------|--------------------------|--------------------------|
| 5 | 320 | 7.0×10^8 | 64 | 67 |
| 10 | 640 | 1.2×10^9 | 128 | 148 |
| 25 | 1600 | 2.7×10^9 | 320 | 284 |
| 100 | 6400 | 1.8×10^{10} | 1472 | 1277 |

Note. Here λ counts data separation by data points, $\lambda\tau$ counts data separation by time, $A(0)$ is the correlation function value at zero separation, λ_c^e is the exponential definition of the correlations scale, and λ_c^i is the integration definition of the correlation scale.

in the same manner. Figure 8 shows the resulting correlation function for four different values of the lag, where we use the same technique as was used to produce Figure 7. As with $A(D_3^{\pm})$, the correlation scale is again consistently 20% of the lag value.

This raises the interesting point that the correlation functions of structure functions generally behave as seen in Figures 7 and 8 in that their correlation scale depends on the lag chosen. At the least, we have examined the first- and second-order expressions of the primitive variables (not all shown here) along with the third-order expressions for ϵ , and they all behave in the same manner. This can be understood relatively simply if one examines the autocorrelation function for the second-order expression,

$$A([\Delta Z_R^+(\lambda)]^2, \delta n) = \frac{1}{(N - \delta n - \lambda)} \sum_{n=1}^{N - \delta n - \lambda} \{[\Delta Z_R(n, \lambda)]^2 [\Delta Z_R(n + \delta n, \lambda)]^2\}, \quad (18)$$

where λ is the lag in terms of the variable point count associated with the second-order expression, $L = \lambda\tau V_{\text{SW}}$, and

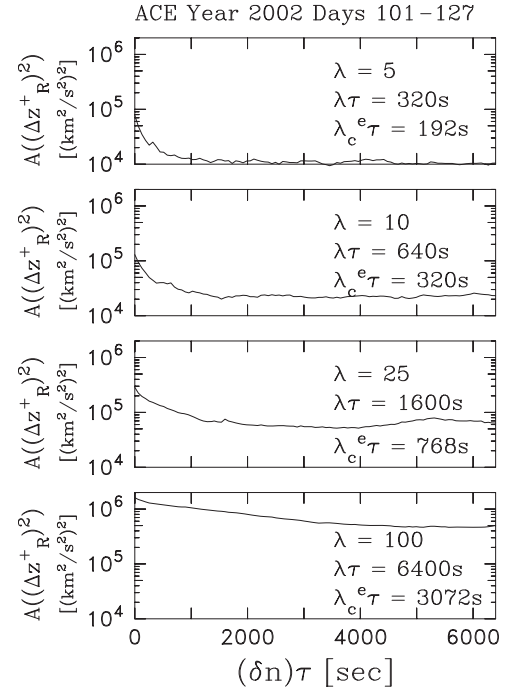


Figure 8. Correlation function for the second-order expression $(\Delta Z_R^+)^2$ evaluated at the same four lags as in Figure 7. Note that the correlation scale again tracks with the lag used in each analysis.

δn is again the variable associated with the lag in the computed autocorrelation function. The two terms that form the argument of the summation provide the greatest reinforcement when $\delta n \leq \lambda$. If $\delta n \gg \lambda$, the two differences are significantly out of phase as they sum across the time series, and this results in decorrelation. For the mixed, third-order expressions above that are not positive in the manner that the second-order expression

is seen to be, this decorrelation includes outright cancellation in much the same way that two sine functions are orthogonal to each other under appropriate integration. If δn is sufficiently small, the two terms are nearly identical, and there is no cancellation.

What is important to remember is that the expressions for the energy cascade rate were derived from the dynamical equations in a general manner that did not select specific nonlinear processes or wave modes. It is a general aspect of the MHD equations that expressions describing the nonlinear transport of energy in the inertial range are third-order structure functions, and these expressions possess a lag-dependent correlation scale. It therefore follows that this is a characteristic of the cascade and thereby more significant than being simply a property of the autocorrelation of structure functions generally.

4. Discussion

We have examined the correlation function for mixed, third-order expressions that can be derived as general equations for the energy cascade in incompressible MHD turbulence. These expressions are highly general and derived without relying on a specific underlying cascade dynamic. The corresponding HD expressions that describe the energy cascade in the inertial range have been shown to yield rates that are closely correlated with dissipation rates (Stolovitzky et al. 1992). The MHD forms have been shown to yield energy cascade rates that agree with thermal proton heating rates in the solar wind at 1 au (Stawarz et al. 2009; Coburn et al. 2012) and at higher latitudes (Marino et al. 2012) when averaged over suitable ensembles. The sample sizes used in our earlier papers (1–12 hr) were comparable to or exceeded the correlation scales for the primitive variables. This was assumed to be adequate to justify the use of Gaussian statistics in describing uncertainties in those analyses. In view of the results shown here, such long intervals represent many correlation scales for the cascade dynamics. Still, many such intervals were required for the average to converge to a mean that is consistent with the observed average heating rate and with scalings predicted by theories derived from the power spectrum (Vasquez et al. 2007). The convergence analysis shown in Table 3 and the distributions shown in Figure 5 offer partial explanations for the slow convergence. Examination of the statistical variations of the third-order expressions averaged over 1–3 hr intervals (Coburn et al. 2014, 2015) still shows large variations in the computed cascade rates. In both cases, the majority of the third-order averages computed over 1–3 hr intervals were seen to scale linearly with lag, as predicted by theory. The statistical variability is seen both here and in Coburn et al. (2014, 2015) to have a standard deviation $\sim 10\times$ larger than the mean of the distribution, which is the quantity that compares favorably with the local heating rates. This means that in almost half of the observations, the inferred energy cascade rate is negative. Without a significant energy source at small scales, it is difficult to imagine how the solar wind turbulent cascade could maintain energy transport from small to large scales.

We have taken care to distinguish between Equations (8) and (9) and other expressions like them, where one involves an ensemble average and one does not. The quantities that have been derived to describe the turbulent cascade of energy all involve ensemble averages. This is why we use language such as “third-order expression” that forms the basis for our analysis instead of “third moment,” which requires an ensemble

average. Inherently, we are assuming that the ensemble average needed to satisfy the derivation of third-moment expressions such as Equations (9) and (16) commutes with the average contained within the correlation functions, but this is unproven.

This analysis indicates that the energy cascade rate is not correlated from one sample to another and that it decorrelates at the scale of interest. Therefore, if L is a scale within the inertial range, the cascade at one point in the fluid is decorrelated from the cascade in less than a distance L away. If the scale $L/10$ is also within the inertial range, it decorrelates at a distance $L/10$. This suggests that the instantaneous cascade rate at any point in space and time is not uniform across the inertial-range scales and that the cascades at the various scales are likely to be uncorrelated with one another. This motivates a view of inertial-range dynamics where the separate scales are independently transporting energy, with the net transport of energy from large to small scales being only a long-term average result and not a reliably instantaneous description of the turbulence. While we have not employed the traditional analysis of higher-order structure functions, this form of patchy and highly variable energy cascade could be described as intermittent (Monin & Yaglom 1971; Sreenivasan & Antonia 1997).

5. Summary

We have used *ACE* magnetic field and thermal proton data to compute the autocorrelation function for third-order expressions that were previously derived as equations for the rate of energy transport through the turbulent spectrum. One solar rotation of data was employed with the removal of shocks, their foreshocks, and driver gas. For comparison, we also compute the autocorrelation function for the primitive variables (magnetic field, solar wind velocity, proton density, and temperature) using techniques that are comparable to previous analyses. While the primitive variables possess correlation scales that vary with the definition of the mean, the third-order structure functions that yield rigorous definitions for the turbulent cascade rate possess lag-dependent correlation scales. Correlation scales for structure functions are consistently $\sim 20\%$ of the lag value, where the lag value is the scale size of interest. This means that the cascade dynamics associated with the larger scales of the turbulent inertial range remain coherent over comparably large scales, while the smaller scales decorrelate over relatively small scales. When combined with the observation that the cascade rates are almost equally positive and negative, the conclusion is that separate scales within the turbulent inertial range act independently, with the net transport of energy from large to small scales resulting only as the average behavior, which is by no means steady-state. The transport of energy within the inertial range is a highly variable, scale-dependent process that only results in the heating of thermal particles over relatively long time averages.

The authors thank the *ACE*/SWEPAM team for providing the thermal proton data used in this study. C.W.S. is supported by Caltech subcontract 44A-1062037 to the University of New Hampshire in support of the *ACE*/MAG instrument. C.W.S., B.J.V., and M.A.F. are supported by NSF/SHINE grant 1622413 to the University of New Hampshire. J.T.C. is a graduate student at Università della Calabria. Data used here can be obtained at the *ACE* Science Center and National Space Science Data Center. The shocks identified in this study are described at http://www.ssg.sr.unh.edu/mag/ace/ACELists/obs_list.html and are available

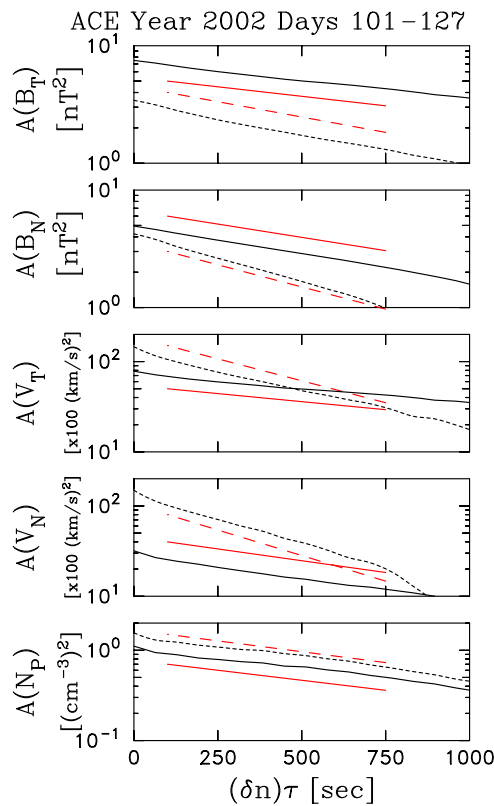




Figure 9. Several panels reproduced from Figure 2 with a logarithmic vertical axis. The red lines are drawn with the fit values of λ_c^e , offset from the curves for clarity. The computed correlation functions are well described as exponential functions at scales up to 1000 s and well fit by λ_c^e . At longer separations, the computed functions turn down and eventually become negative. Beyond this point, they do not demonstrate exponential forms.

online through the ACE Science Center. The authors wish to thank Prof. Sean Oughton at the University of Waikato for a very useful discussion.

Appendix Exponential Correlation Functions

Above, we adopt the tradition of showing correlation functions on linear scalings so that the reader may see that the correlation functions cross zero, which is of interest in some discussions. However, it is worth demonstrating that the correlation functions also exhibit an exponential scaling in the inertial range, and that our method for finding λ_c^e accurately reproduces that exponential form. Figure 9 gives several of the panels from Figure 2 with a logarithmic vertical axis. The red lines possess the computed λ_c^e for slopes and are offset from the curves for clarity. Note that λ_c^e yields a good description of the correlation functions at these scales.

ORCID iDs

Charles W. Smith  <https://orcid.org/0000-0002-5379-1542>
Bernard J. Vasquez  <https://orcid.org/0000-0001-8593-7289>

References

Adhikari, L., Zank, G. P., Bruno, R., et al. 2015a, *ApJ*, 805, 63
Adhikari, L., Zank, G. P., Bruno, R., et al. 2015b, *J. Physics: Conf. Series*, 642, 012001
Alexandrova, O., Bale, S. D., & Lacombe, C. 2013, *PhRvL*, 111, 149001

Alexandrova, O., Saur, J., Lacombe, C., et al. 2009, *PhRvL*, 103, 165003
Bale, S. D., Kellogg, P. J., Mozer, F. S., Horbury, T. S., & Reme, H. 2005, *PhRvL*, 94, 215002
Batchelor, G. K. 1953, *The Theory of Homogeneous Turbulence* (New York: Cambridge Univ. Press)
Behannon, K. W. 1978, *RvGeo*, 16, 125
Belcher, J. W., & Davis, L., Jr. 1971, *JGR*, 76, 3534
Boldyrev, S. 2005, *ApJ*, 626, L37
Boldyrev, S. 2006, *PhRvL*, 96, 115002
Bourouaine, S., Alexandrova, O., Marsch, E., & Maksimovic, M. 2012, *ApJ*, 749, 102
Boyd, T. J., & Sanderson, J. J. 1969, *Plasma Dynamics* (New York: Barnes and Noble)
Breech, B., Matthaeus, W. H., Cranmer, S. R., Kasper, J. C., & Oughton, S. 2009a, *JGR*, 114, A09103
Breech, B., Matthaeus, W. H., Minnie, J., et al. 2005, *GeoRL*, 32, L06103
Breech, B., Matthaeus, W. H., Minnie, J., et al. 2008, *JGR*, 113, A08105
Breech, B., Matthaeus, W. H., Minnie, J., et al. 2009b, *JGR*, 114, A09103
Bruno, R., & Carbone, V. 2013, *LRSP*, 10, 2
Burlaga, L. F. 1991, *JGR*, 96, 5847
Chen, C. H. K., Leung, L., Boldyrev, S., Maruca, B. A., & Bale, S. D. 2014, *GeoRL*, 41, 8081
Coburn, J. T., Forman, M. A., Smith, C. W., Vasquez, B. J., & Stawarz, J. E. 2015, *RSPTA*, 373, 20140150
Coburn, J. T., Smith, C. W., Vasquez, B. J., Forman, M. A., & Stawarz, J. E. 2014, *ApJ*, 786, 52
Coburn, J. T., Smith, C. W., Vasquez, B. J., Stawarz, J. E., & Forman, M. A. 2012, *ApJ*, 754, 93
Coleman, P. J., Jr. 1966, *PhRvL*, 17, 207
Coleman, P. J., Jr. 1968, *ApJ*, 153, 371
Dasso, S., Matthaeus, W. H., Weygand, J. M., et al. 2008, *Proc. ICRC (Universidad Nacional Autónoma de México)*, 1, 625
Elsässer, W. M. 1950, *PhRv*, 79, 183
Fisk, L. A., & Sari, J. W. 1973, *JGR*, 78, 6729
Forman, M. A., Smith, C. W., & Vasquez, B. J. 2010, *PhRvL*, 104, 189001
Garrard, T. L., Davis, A. J., Hammond, J. S., & Sears, S. R. 1998, *SSRv*, 86, 649
Goldreich, P., & Sridhar, S. 1995, *ApJ*, 438, 763
Goldstein, M. L., Roberts, D. A., & Fitch, C. A. 1994, *JGR*, 99, 11519
Hadid, L. Z., Sahraoui, F., & Galtier, S. 2017, *ApJ*, 838, 9
Hamilton, K., Smith, C. W., Vasquez, B. J., & Leamon, R. J. 2008, *JGR*, 113, A01106
Higdon, J. C. 1984, *ApJ*, 285, 109
Iroshnikov, P. S. 1964, *SvA*, 7, 566
Isenberg, P. A. 2005, *ApJ*, 623, 502
Isenberg, P. A., Smith, C. W., & Matthaeus, W. H. 2003, *ApJ*, 592, 564
Isenberg, P. A., Smith, C. W., Matthaeus, W. H., & Richardson, J. D. 2010, *ApJ*, 719, 716
Kolmogorov, A. N. 1941a, *DoSSR*, 30, 301
Kolmogorov, A. N. 1941b, *DoSSR*, 32, 16
Kolmogorov, A. N. 1962, *JFM*, 13, 82
Kraichnan, R. H. 1965, *PhFl*, 8, 1385
Leamon, R. J., Matthaeus, W. H., Smith, C. W., et al. 2000, *ApJ*, 537, 1054
Leamon, R. J., Matthaeus, W. H., Smith, C. W., & Wong, H. K. 1998a, *ApJ*, 507, L181
Leamon, R. J., Smith, C. W., & Ness, N. F. 1998b, *GeoRL*, 25, 2505
Leamon, R. J., Smith, C. W., Ness, N. F., Matthaeus, W. H., & Wong, H. K. 1998c, *JGR*, 103, 4775
Leamon, R. J., Smith, C. W., Ness, N. F., & Wong, H. K. 1999, *JGR*, 104, 22331
MacBride, B. T., Forman, M. A., & Smith, C. W. 2005, in *Proc. Solar Wind 11: Connecting Sun and Heliosphere*, ESA SP-592, ed. B. Fleck & T. H. Zurbuchen (The Netherlands: European Space Agency), 613
MacBride, B. T., Smith, C. W., & Forman, M. A. 2008, *ApJ*, 679, 1644
MacBride, B. T., Smith, C. W., & Vasquez, B. J. 2010, *JGR*, 115, A07105
Marino, R., Sorisso-Valvo, L., Carbone, V., et al. 2008, *ApJL*, 677, L71
Marino, R., Sorisso-Valvo, L., Carbone, V., et al. 2011, *P&SS*, 59, 592
Marino, R., Sorisso-Valvo, L., D'Amicis, R., et al. 2012, *ApJ*, 750, 41
Markovskii, S. A., Vasquez, B. J., & Smith, C. W. 2008, *ApJ*, 675, 1576
Matthaeus, W. H., Dasso, S., Weygand, J. M., et al. 2005, *PhRvL*, 95, 231101
Matthaeus, W. H., Dasso, S., Weygand, J. M., Kivelson, M. G., & Osman, K. T. 2010, *ApJL*, 721, L10
Matthaeus, W. H., & Goldstein, M. L. 1982, *JGR*, 87, 6011
Matthaeus, W. H., & Goldstein, M. L. 1986, *PhRvL*, 57, 495
Matthaeus, W. H., Goldstein, M. L., & Roberts, D. A. 1990, *JGR*, 95, 20673
Matthaeus, W. H., Oughton, S., Pontius, D., & Zhou, Y. 1994, *JGR*, 99, 19267
Matthaeus, W. H., Smith, C. W., & Bieber, J. W. 1999, in *AIP Conf. Proc.* 471, *Solar Wind 9*, ed. S. R. Habbal et al. (College Park, MD: AIP), 511

- Matthaeus, W. H., & Velli, M. 2011, *SSRv*, **160**, 145
- Matthaeus, W. H., Zank, G. P., Smith, C. W., & Oughton, S. 1999, *PhRvL*, **82**, 3444
- McComas, D. J., Bame, S. J., Barker, P., et al. 1998, *SSRv*, **86**, 563
- Monin, A. S., & Yaglom, A. M. 1971, *Statistical Fluid Mechanics: Mechanics of Turbulence*, Vol. 1 (Cambridge, MA: MIT Press)
- Narita, Y., Gary, S. P., Saito, S., Glassmeier, K.-H., & Motschmann, U. 2011, *GeoRL*, **38**, L05101
- Ng, C. S., Bhattacharjee, A., Munsri, D., Isenberg, P. A., & Smith, C. W. 2010, *JGR*, **115**, A02101
- Oughton, S., Matthaeus, W. H., Smith, C. W., Breech, B., & Isenberg, P. A. 2011, *JGR*, **116**, A08105
- Parker, E. N. 1961, in *Science in Space*, ed. L. V. Berkner & H. Odishaw (New York: McGraw-Hill), 138
- Parker, E. N. 1963, *Interplanetary Dynamical Processes* (New York: Wiley-Interscience)
- Podesta, J. J., Forman, M. A., Smith, C. W., Elton, D. C., & Malécot, Y. 2009, *NPGeo*, **16**, 99
- Politano, H., & Pouquet, A. 1998a, *PhRvE*, **57**, R21
- Politano, H., & Pouquet, A. 1998b, *GeoRL*, **25**, 273
- Roberts, O. W., Li, X., & Jeska, J. 2015, *ApJ*, **802**, 2
- Roberts, O. W., Narita, Y., Li, X., Escoubet, C. P., & Laakso, H. 2017, *JGR*, **122**, 6940
- Sahraoui, F., Goldstein, M. L., Belmont, G., Canu, P., & Rezeau, L. 2010, *PhRvL*, **105**, 131101
- Sahraoui, F., Goldstein, M. L., Robert, P., & Khotyaintsev, Yu. V. 2009, *PhRvL*, **102**, 231102
- Shebalin, J. V., Matthaeus, W. H., & Montgomery, D. 1983, *JPIPh*, **29**, 525
- Smith, C. W. 2009, in *Heliophysics I. Plasma Physics of the Local Cosmos*, ed. C. J. Schrijver & G. Siscoe (Cambridge: Cambridge Univ. Press) Chapter 7
- Smith, C. W., Acuña, M. H., Burlaga, L. F., et al. 1998, *SSRv*, **86**, 613
- Smith, C. W., Hamilton, K., Vasquez, B. J., & Leamon, R. J. 2006a, *ApJL*, **645**, L85
- Smith, C. W., Isenberg, P. A., Matthaeus, W. H., & Richardson, J. D. 2006b, *ApJ*, **638**, 508
- Smith, C. W., Matthaeus, W. H., Zank, G. P., et al. 2001a, *JGR*, **106**, 8253
- Smith, C. W., Mullan, D. J., Ness, N. F., Skoug, R. M., & Steinberg, J. 2001b, *JGR*, **106**, 18625
- Smith, C. W., Stawarz, J. E., Vasquez, B. J., Forman, M. A., & MacBride, B. T. 2009, *PhRvL*, **103**, 201101
- Smith, C. W., Stawarz, J. E., Vasquez, B. J., Forman, M. A., & MacBride, B. T. 2010, *PhRvL*, **104**, 169002
- Smith, C. W., Tessein, J. A., Vasquez, B. J., & Skoug, R. M. 2011, *JGR*, **116**, A10103
- Smith, C. W., Vasquez, B. J., & Hollweg, J. V. 2012, *ApJ*, **745**, 8
- Sorriso-Valvo, L., Carbone, V., Veltri, P., Consolini, G., & Bruno, R. 1999, *GeoRL*, **26**, 1801
- Sorriso-Valvo, L., Marino, R., Carbone, V., et al. 2007, *PhRvL*, **99**, 115001
- Sreenivasan, K. R., & Antonia, R. A. 1997, *AnRFM*, **29**, 435
- Stawarz, J. E., Smith, C. W., Vasquez, B. J., Forman, M. A., & MacBride, B. T. 2009, *ApJ*, **713**, 920
- Stawarz, J. E., Smith, C. W., Vasquez, B. J., Forman, M. A., & MacBride, B. T. 2010, *ApJ*, **697**, 1119
- Stawarz, J. E., Vasquez, B. J., Smith, C. W., Forman, M. A., & Klewicki, J. 2011, *ApJ*, **736**, 44
- Stolovitzky, G., Kailasnath, P., & Sreenivasan, K. R. 1992, *PhRvL*, **69**, 1178
- Stone, E. C., Frandsen, A. M., Mewaldt, R. A., et al. 1998, *SSRv*, **86**, 1
- Szabo, A. 1994, *JGR*, **99**, 14737
- Taylor, G. I. 1938, *RSPSA*, **164**, 476
- Tessein, J. A., Smith, C. W., MacBride, B. T., et al. 2009, *ApJ*, **692**, 684
- Tessein, J. A., Smith, C. W., Vasquez, B. J., & Skoug, R. M. 2011, *JGR*, **116**, A10104
- Usmanov, A. V., & Goldstein, M. L. 2006, *JGR*, **111**, A07101
- Usmanov, A. V., Goldstein, M. L., & Matthaeus, W. H. 2012, *ApJ*, **754**, 40
- Usmanov, A. V., Goldstein, M. L., & Matthaeus, W. H. 2014, *ApJ*, **788**, 43
- Usmanov, A. V., Goldstein, M. L., & Matthaeus, W. H. 2016, *ApJ*, **820**, 17
- Usmanov, A. V., Matthaeus, W. H., Breech, B. A., & Goldstein, M. L. 2011, *ApJ*, **727**, 84
- Vasquez, B. J., Smith, C. W., Hamilton, K., MacBride, B. T., & Leamon, R. J. 2007, *JGR*, **112**, A07101
- Viñas, A. F., & Scudder, J. D. 1986, *JGR*, **91**, 39
- von Karman, T., & Howarth, L. 1938, *RSPSA*, **164**, 192
- Vorotnikov, V. S., Smith, C. W., Farrugia, C. J., et al. 2011, *SpWea*, **9**, S04001
- Vorotnikov, V. S., Smith, C. W., Hu, Q., et al. 2008, *SpWea*, **6**, S03002
- Yaglom, A. 1949, *DoSSR*, **69**, 743
- Zank, G. P., Dosch, A., Hunana, P., et al. 2012, *ApJ*, **745**, 35
- Zank, G. P., Matthaeus, W. H., & Smith, C. W. 1996, *JGR*, **101**, 17093
- Zhou, Y., & Matthaeus, W. H. 1989, *GeoRL*, **16**, 755
- Zhou, Y., & Matthaeus, W. H. 1990a, *JGR*, **95**, 10291
- Zhou, Y., & Matthaeus, W. H. 1990b, *JGR*, **95**, 14881